



## Enhancement for the fluorescent properties of new synthesized GFPs chromophore

Bahaa Elgendy, M. M. Azab, Marwa Gamil, and Hesham H. El-Feky\*.  
Chemistry department, faculty of science, Benha University, Egypt



### Abstract

An alternative method for the synthesis of new GFP chromophore analogous that possess good photo physical properties which can be used as efficient biomarkers. These compounds have low fluorescence most probably due to their Z-E photo isomerization. These chromophores have suitable site for complexation with transitional metals. Forming complexes with metal ions can inhibit their photo isomerization and enhance the fluorescent properties.

**Keywords:** GFP chromophore; Z-E isomerization; complexes

### 1. Introduction

In recent decades, green fluorescent protein (GFP) was discovered ago. include 238 amino acid residues with a  $\beta$ -barrel structure.<sup>1-6</sup> Shimomura et al<sup>7-10</sup> purified and characterized the first light-producing protein from the jellyfish *Aequorea victoria*. Osamu Shimomura, Martin Chalfie and Roger Tsien award 2008 Nobel Prize in chemistry for the discovery and isolation of (GFP).<sup>11</sup> Tsien and coworkers put forward the bioluminescence principle of GFP, indicating that the GFP chromophore is formed via the autocatalytic oxidation/dehydration process of a Ser65-Tyr66-Gly67 motif.<sup>12-14</sup> when GFP chromophore removed from the  $\beta$ -barrel protein system either by denaturation or by independent synthesis, it become nonfluorescent.<sup>15</sup> This is most likely due to an internal conversion mechanism induced by twisting in the excited state, like a cis/trans isomerization pathways.<sup>16</sup> Previous studies suggest that the absorbed energy is used in torsional motions to produce the E-Isomer instead of producing the green light.<sup>17</sup>

#### Restoring the Chromophore Fluorescence

There are many published papers that discuss different techniques to restore the fluorescence<sup>18</sup> of the denaturated or the synthesized chromophore either using Lewis acid as  $\text{BF}_3$ , or by metal complexation,<sup>19</sup> or by using intramolecular hydrogen bond.

#### Using Metal Complexes

Metal ion locking will greatly 'turn-on' the emission of GFPc analogs, which can be applied to fabricate metal ion sensors.<sup>20</sup> For example, Baldrige et al.<sup>21</sup> developed  $\text{Zn}^{2+}$  sensors with good selectivity and sensitivity using chromophore. To improve its binding ability and stability, Fang et al.<sup>22-24</sup>

**Synthesis of chromophore** is started with synthesizing of oxazolinone<sup>23,24</sup> then The oxazolinone ring opening reaction was examined with a variety of ammonia source compounds followed by the subsequent 3,5-dihydro-imidazol-4-one cyclization reaction, which was carried out with either an organic or inorganic base in aprotic solvents.<sup>27,28</sup> Imidazole with NH group is reacted with acetic anhydride to give the acetyl<sup>29</sup> product GFP chromophore.

#### 2. Experimental Section

**General Remarks:** All the reagents were commercial grade and purified according to established procedures. Organic extracts were dried with anhydrous sodium sulfate. Reactions were monitored by TLC on silica-gel 60 F254 (0.25 mm) as a stationary phase. Melting points were recorded. All the compounds were identified and confirmed by IR and NMR spectroscopy and by comparison with authentic samples.

#### **Synthesis of imidazolinone (3,5-dihydro-imidazol-4-one) By using ammonium acetate:**

A mixture of (Z)-2-phenyl-4-(thiophen-2-ylmethylene) oxazol-5(4H)-one (4 mmol, 1.02 gm),

\*Corresponding author e-mail: [hesham.elfeky@fsc.bu.edu.eg](mailto:hesham.elfeky@fsc.bu.edu.eg), mobile: 00201060204453).

Receive Date: 07 April 2021, Revise Date: 17 April 2021, Accept Date: 18 April 2021

DOI: 10.21608/EJCHEM.2021.71465.3569

©2021 National Information and Documentation Center (NIDOC)

ammonium acetate (2.4 mmol, 0.18 gm), and DMF (4 mL) was stirred at room temperature. Triethylamine (4 mmol, 0.34 mL) was added and the mixture was slowly heated to 55 °C for 30 min. Potassium carbonate (2 mmol, 0.26 gm) was added to the solution, and the temperature increased to 90-93 °C for 12 h. The color of the reaction changed from turbid to clear. Upon reaction completion, confirmed by TLC, the mixture was cooled to 60–65 °C, and water was added dropwise while keeping the temperature >60 °C. Then slowly cooled to room temperature. The precipitate formed was filtered and washed with cold water to give the corresponding imidazolinone in good yields(91%) Scheme 1.

**[3a] (Z)-5-(4-chlorobenzylidene)-2-phenyl-3,5-dihydro-4H-imidazol-4-one**

Yellow precipitate m.p. 270-271 °C lit. (268–269 °C); Rf= 0.69 (EtOAc / Hexane 1:4). IR (KBr)  $\nu_{\max}$  3123  $\text{cm}^{-1}$  (NH), 1701.8  $\text{cm}^{-1}$  (C=O), 1647.3  $\text{cm}^{-1}$  (C=N), 1514  $\text{cm}^{-1}$  (C=C) Fig. 1.

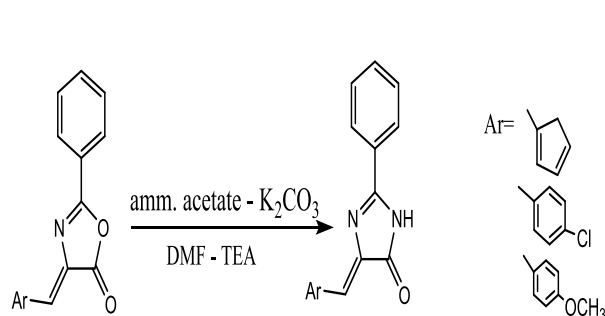
**[3b] (Z)-5-(4-methoxybenzylidene)-2-phenyl-3,5-dihydro-4H-imidazol-4-one**

Yellow precipitate m.p. (286-288 °C) lit. (292–294 °C); Rf= 0.65 (EtOAc / Hexane 1:4). IR (KBr)  $\nu_{\max}$  3184  $\text{cm}^{-1}$  (NH), 1701.8  $\text{cm}^{-1}$  (CO), 1635.9  $\text{cm}^{-1}$  (C=N), 1512.3  $\text{cm}^{-1}$  (C=C) Fig 2.

**[3c] (Z)-2-phenyl-5-(thiophen-2-ylmethylene)-3,5-dihydro-4H-imidazol-4-one**

Yellow precipitate (91% yield); m.p. 300-302°C lit. (310-311 °C); Rf= 0.36 (EtOAc / Hexane 1:4). IR (KBr)  $\nu_{\max}$  3291  $\text{cm}^{-1}$  (NH), 1698.4  $\text{cm}^{-1}$  (C=O), 1647.89  $\text{cm}^{-1}$  (C=N), 1587  $\text{cm}^{-1}$  (C=C) Fig 3.

**[3d](Z)-5-(4-(dimethylamino)benzylidene)-2-phenyl-3,5-dihydro-4H-imidazol-4-one**



scheme(1) Synthesis of 3,5-dihydro-4H-imidazol-4-one (3a-d)

Red precipitate m.p. 260 - 262 °C; Rf= 0.78 (EtOAc / Hexane 1:4). IR (KBr)  $\nu_{\max}$  3181  $\text{cm}^{-1}$  (NH), 1784  $\text{cm}^{-1}$  (CO), 1647  $\text{cm}^{-1}$  (C=N), 1530.5  $\text{cm}^{-1}$  (C=C) Fig 4.

**Synthesis of acetyl derivatives of imidazolinone:**

A mixture of (Z)-2-phenyl-5-(thiophen-2-ylmethylene)-3,5-dihydro-4H-imidazol-4-one (0.5 mmol, 0.15 gm) and Acetic anhydride (1 mL) was heated to 95 °C for 24 h. After reaction completion, water was added. The precipitate formed was filtered and washed with water to give the corresponding imidazolinone in good yields (95%) Scheme 2.

**[4a] (Z)-3-acetyl-5-(4-chlorobenzylidene)-2-phenyl-3,5-dihydro-4H-imidazol-4-one**

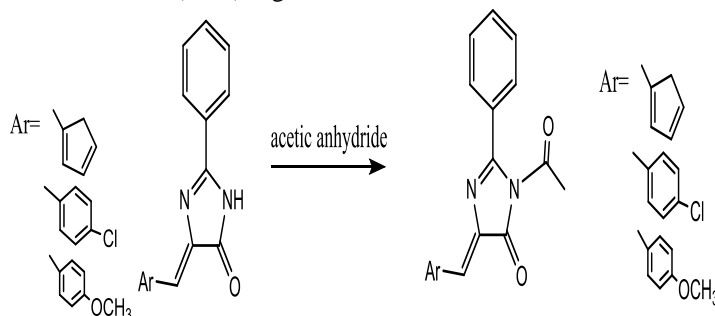
Pale yellow fluffy crystals (55%); m.p 180-182 °C; Rf= 0.86 (EtOAc / Hexane 1:2). <sup>1</sup>H NMR (400 MHz, DMSO)  $\delta$  8.34 (d, 2H), 8.15 (d, 2H), 7.74 (t, 1H), 7.63 (dd, 4H), 7.37 (s, 1H), 3.36 (s, 1H), 3.52 (s, 1H). IR (KBr)  $\nu_{\max}$  1796  $\text{cm}^{-1}$  (CO), 1693  $\text{cm}^{-1}$  (CO), 1654  $\text{cm}^{-1}$  (C=N), 1589  $\text{cm}^{-1}$  (C=C) Fig 5(a, b).

**[4b] (Z)-3-acetyl-5-(4-methoxybenzylidene)-2-phenyl-3,5-dihydro-4H-imidazol-4-one**

Bright Yellow fluffy crystals (49%); m.p 178 – 180 °C; Rf= 0.76 (EtOAc / Hexane 1:2). <sup>1</sup>H NMR (400 MHz, Chloroform-d)  $\delta$  8.23 – 8.18 (m, 2H), 7.64 – 7.52 (m, 2H), 7.28 (d, 1H), 7.01 (d, 1H), 3.92 (s, 1H), 1.6 (s, 1H), 1.27 (s, 1H). IR (KBr)  $\nu_{\max}$  1789  $\text{cm}^{-1}$  (CO), 1771  $\text{cm}^{-1}$  (CO), 1654  $\text{cm}^{-1}$  (C=N), 1596  $\text{cm}^{-1}$  (C=C) Fig 6(a, b).

**[4c] (Z)-3-acetyl-2-phenyl-5-(thiophen-2-ylmethylene)-3,5-dihydro-4H-imidazol-4-one**

Yellow fluffy crystals (53%); m.p 219 – 221 °C; Rf= 0.7 (EtOAc / Hexane 1:2). IR (KBr)  $\nu_{\max}$  1791  $\text{cm}^{-1}$  (CO), 1697  $\text{cm}^{-1}$  (CO), 1641  $\text{cm}^{-1}$  (C=N), 1619  $\text{cm}^{-1}$  (C=C) Fig 7.



scheme(2) Synthesis of acetyl derivatives chromophore (4a-d)

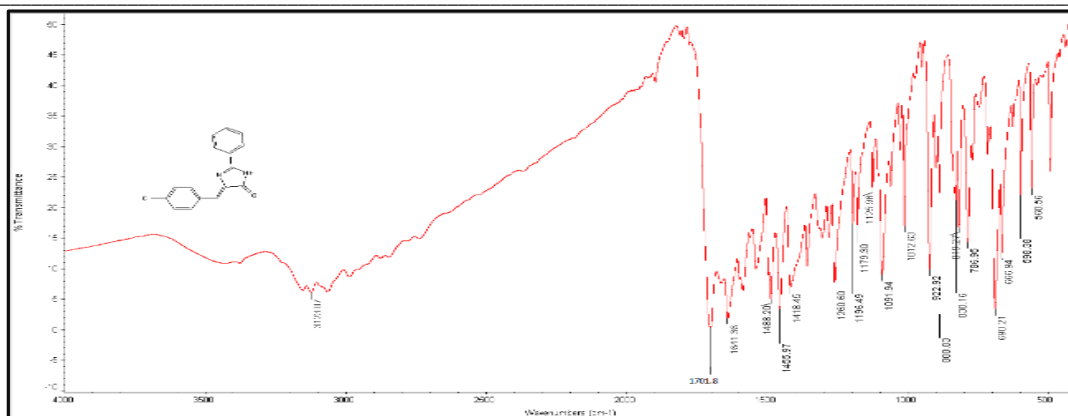


**Fig 1. IR spectra for (Z)-5-(4-chlorobenzylidene)-2-phenyl-3,5-dihydro-4H-imidazol-4-one, [3a].**

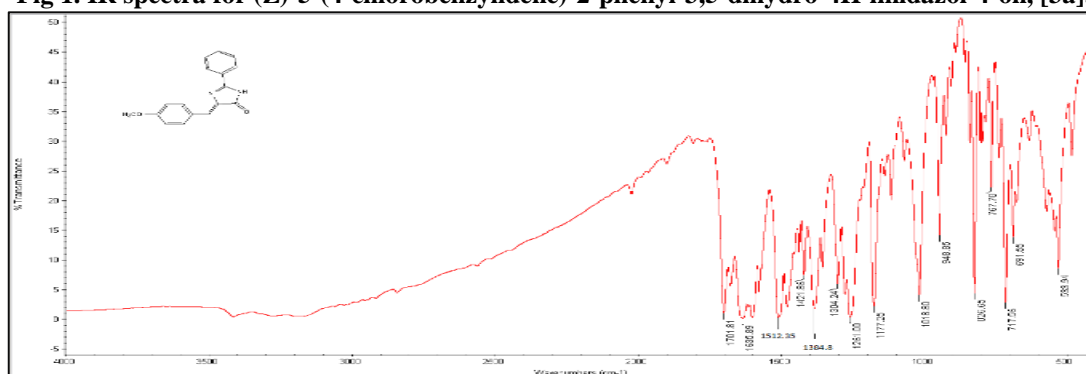


**Fig 2. IR spectra for (Z)-5-(4-methoxybenzylidene)-2-phenyl-3,5-dihydro-4H-imidazol-4-one, [3b].**

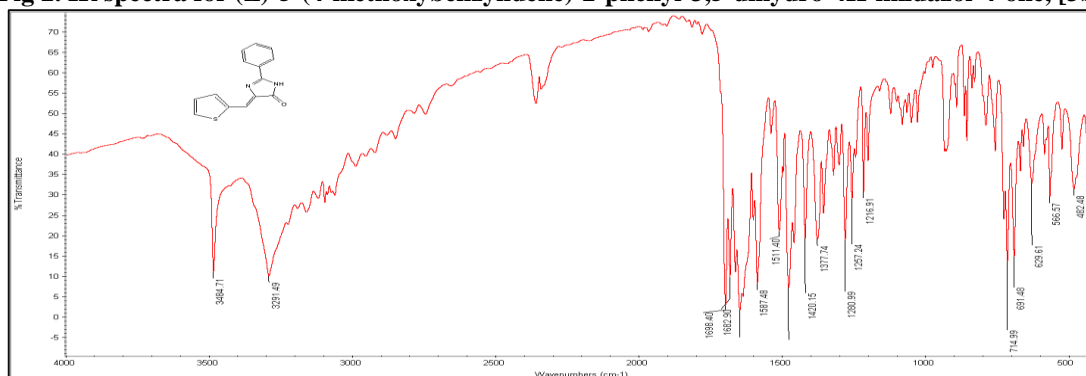


**Fig 3. IR spectra for (Z)-2-phenyl-5-(thiophen-2-ylmethylene)-3,5-dihydro-4H-imidazol-4-one, [3c].**

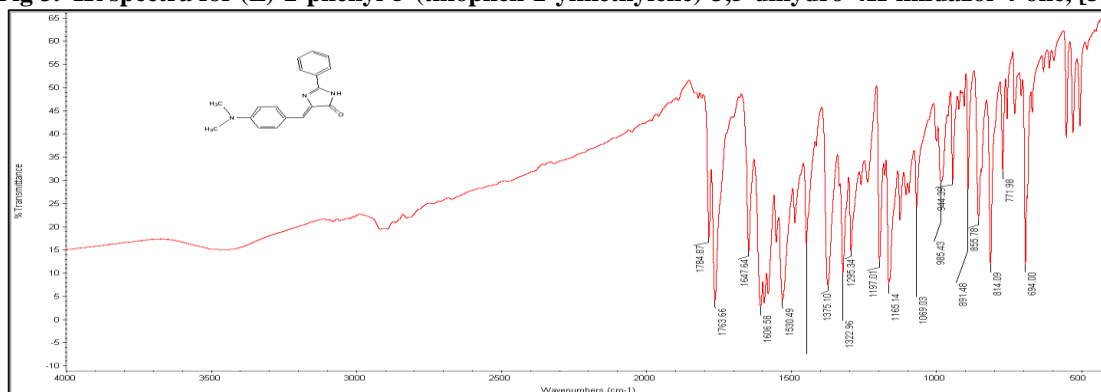


**Fig 4. IR spectra for (Z)-5-(4-(dimethylamino)benzylidene)-2-phenyl-3,5-dihydro-4H-imidazol-4-one, [3d].**

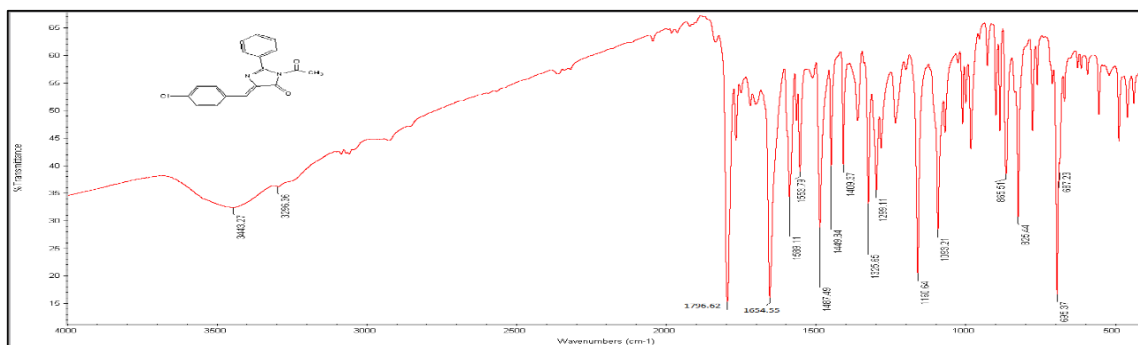


Fig 5(a). IR spectra spectra for (Z)-3-acetyl-5-(4-chlorobenzylidene)-2-phenyl-3,5-dihydro-4H-imidazol-4-one, [4a].

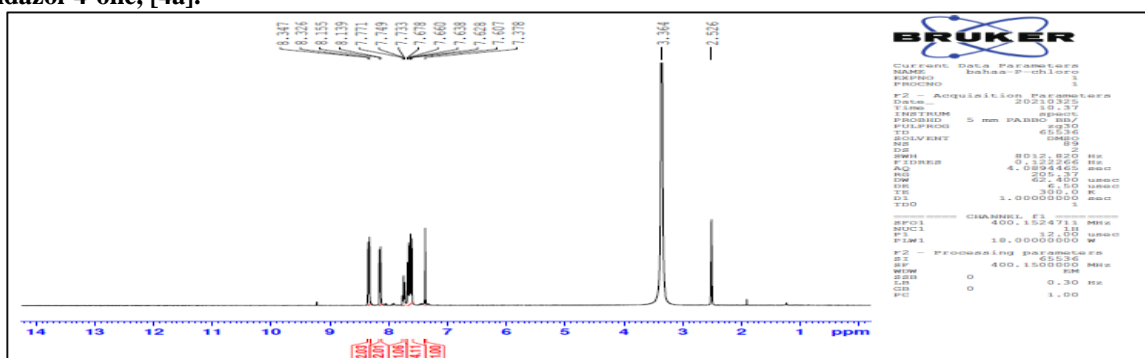


Fig 5(b). NMR spectra for (Z)-3-acetyl-5-(4-chlorobenzylidene)-2-phenyl-3,5-dihydro-4H-imidazol-4-one, [4a].

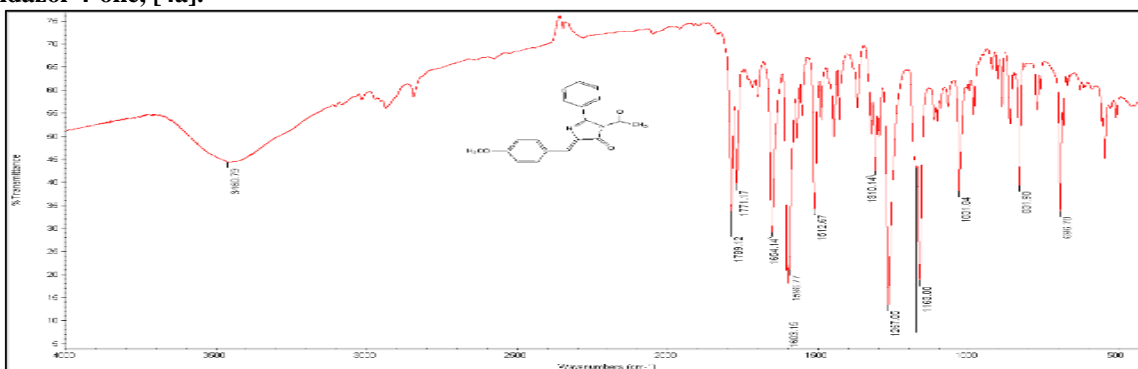


Fig 6 (a). IR spectra spectra for (Z)-3-acetyl-5-(4-methoxybenzylidene)-2-phenyl-3,5-dihydro-4H-imidazol-4-one, [4b].

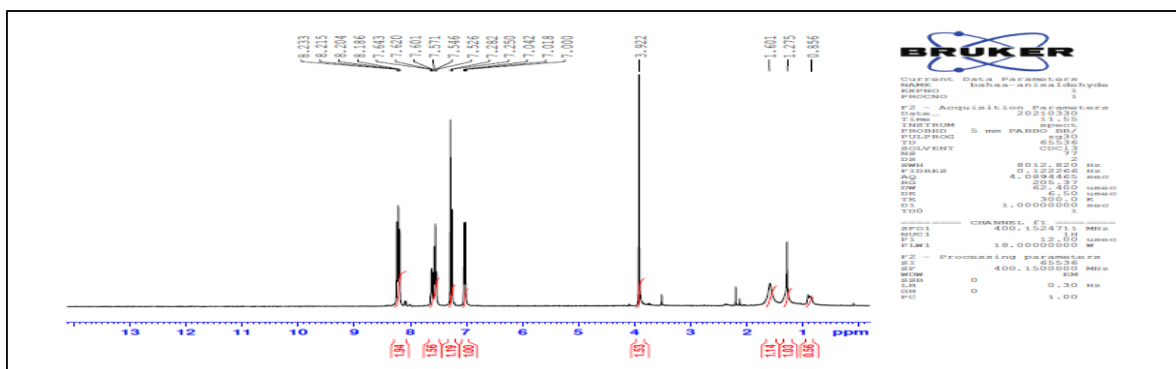


Fig 6 (b). NMR spectra for (Z)-3-acetyl-5-(4-methoxybenzylidene)-2-phenyl-3,5-dihydro-4H-imidazol-4-one, [4b].

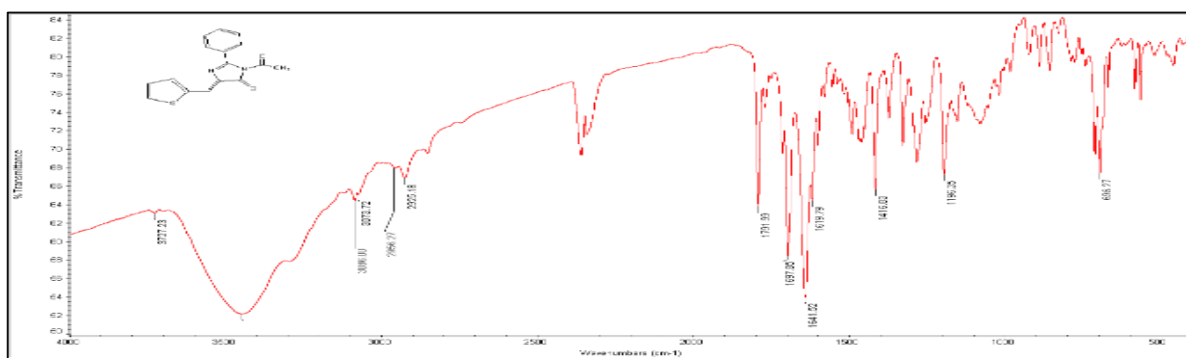


Fig 7. IR spectra for (Z)-3-acetyl-phenyl-5-(thiophen-2-ylmethylene)-3,5-dihydro-4H-imidazol-4-one, [4c].

### 3. Results and Discussion

Cobalt nitrate hexa hydrate is the metal salt that give good complex with ligand(4b, 4c). Synthesized ligands were highly soluble in dichloromethane (DCM) but the metal salt was not. Ligand (4b) moderately soluble in acetonitrile (MeCN), ligand (4c) moderately soluble in ethanol (EtOH) and metal salt (cobalt nitrate) was soluble in both solvents. The (4b) ligand absorbs at 367nm while the complex of this ligand showed bathochromic shift (red shift). It absorbs light at 402nm as shown in Figure (8). The (4c) ligand absorbs at 391 nm and the complex with cobalt showed larger bathochromic shift with absorption peak at 439nm as shown in Figure (9). Thus the formation of the metal complexes can obviously have confirmed by the spectra that detected by uv-visible spectrophotometer (jasco v-670).

#### 3.1. Effect of pH

Studying the effect of factors like pH and amount of buffer were not applicable here due to poor solubility of the ligands in water. The synthesized ligands 4b-c tend to precipitate after adding few drops of buffer.

#### 3.2. Effect of the ligand volume

To study the effect of the volume of the reagents on the complex formation, the volume of the metal ion is kept constant (1.0 mL of  $5.0 \times 10^{-3}$  M), while the volume of the reagent is regularly varied (0.1, 0.2, ..., 0.7 mL of  $5 \times 10^{-3}$  M). The volume was completed with acetonitrile to the mark of 10 mL. The absorption spectrum was recorded against blank solution prepared in the same manner without the metal ion. The absorbance was plotted against mL added of reagent as shown in Fig. 10, 11. The optimum reagent volume for  $\text{Co}^{2+}$ -4b and also for  $\text{Co}^{2+}$ -4c complex was 0.5 mL of  $5 \times 10^{-3}$  M of the reagent for both complexes.

#### 3.3. Effect of time

To determine the optimum conditions required for converting the largest amount of ligand to complex, effect of time was investigated. The Change of intensity of absorbed light was measured at different time intervals. The results of this investigation showed that the intensity of absorbance of ligand (4b) complex increase with time until it reached its highest absorbance after 10 minutes from the addition of the metal solution and then decreased as shown in Fig. 12.

And in case of ligand (4c), the highest absorbance was reached just after 5 minutes after adding the cobalt solution to the 4c solution, then the absorbance decreased with time as shown in Fig. 13.

#### 3.4. Effect of temperature

The effect of temperature was studied for the formed complex by heating the sample and blank solution at different temperatures (25-75 °C). Experiments showed that the highest stability of all complexes was reached at 45 °C, then a decrease in their absorbance occurs. The stability of all formed complexes is decreased by increasing temperature as shown in Figs. 14, 15.

#### 3.5. The stoichiometry of the metal complexes

Investigation of the molecular stoichiometry of complexes formed between  $\text{Co}^{2+}$  ions with ligand 4b or ligand 4c by using a constant metal concentration ( $5 \times 10^{-3}$  M) and varying concentration of ligand (0.2-2.4 mL of  $5 \times 10^{-3}$  M). In the light of the obtained results of molar ratio, the two complexes showed that the molecular stoichiometry of (1:2) and (1:1) (M:L), having the formula of  $\text{ML}$  &  $\text{ML}_2$ . The representation of molar ratio curves are shown in Figs. 16, 17.

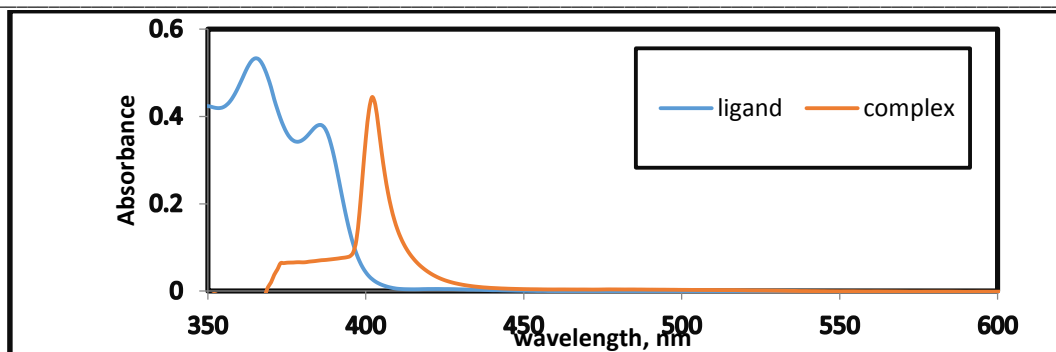


Fig. 8: The difference between the absorption spectra of the ligand (4b) and that of the (4b-Co<sup>+2</sup>) complex.

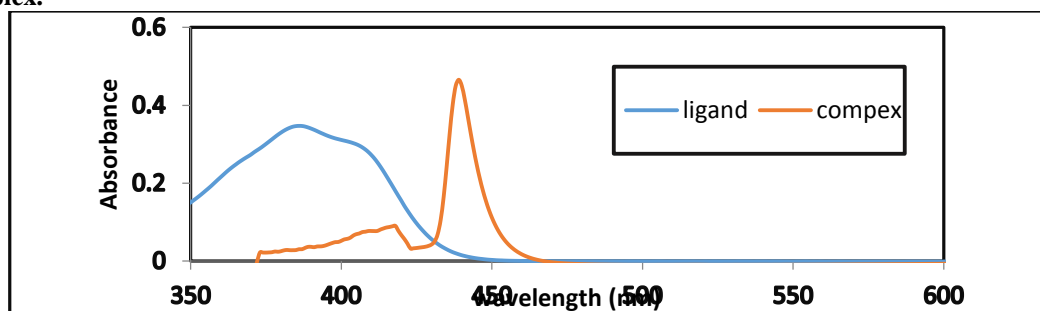


Fig. 9: The difference between the absorption spectra of the ligand (4c) and that of the (4c-Co<sup>+2</sup>) complex

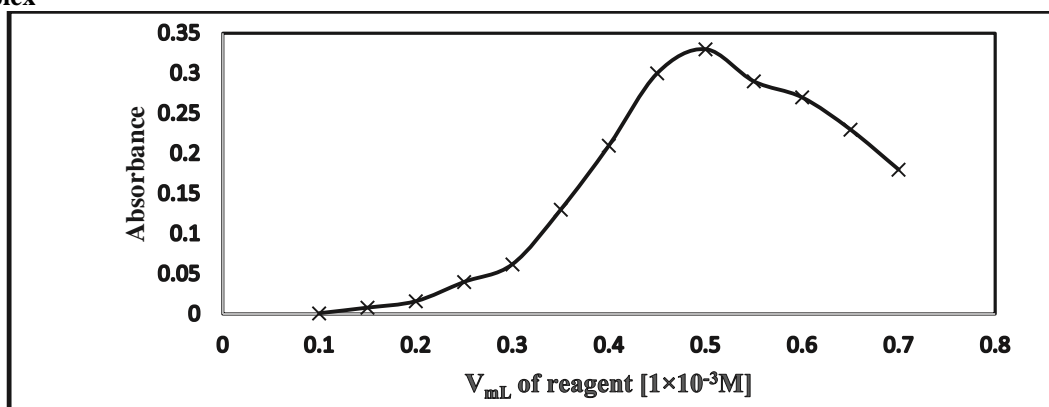


Fig. 10. Effect of the reagent volume 4b on the formed complex of 1.0 mL of  $5 \times 10^{-3}$  M cobalte ion.

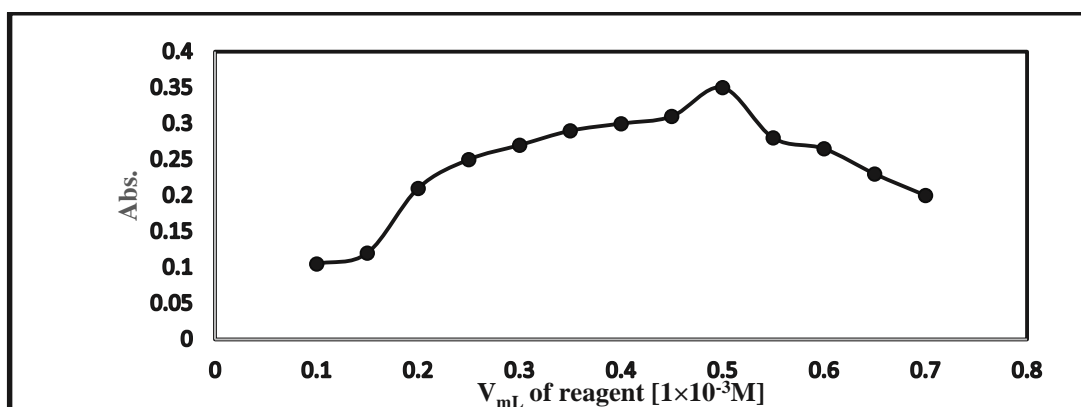


Fig. 11. Effect of the reagent volume 4c on the formed complex of 1.0 mL of  $5 \times 10^{-3}$  M cobalte ion.

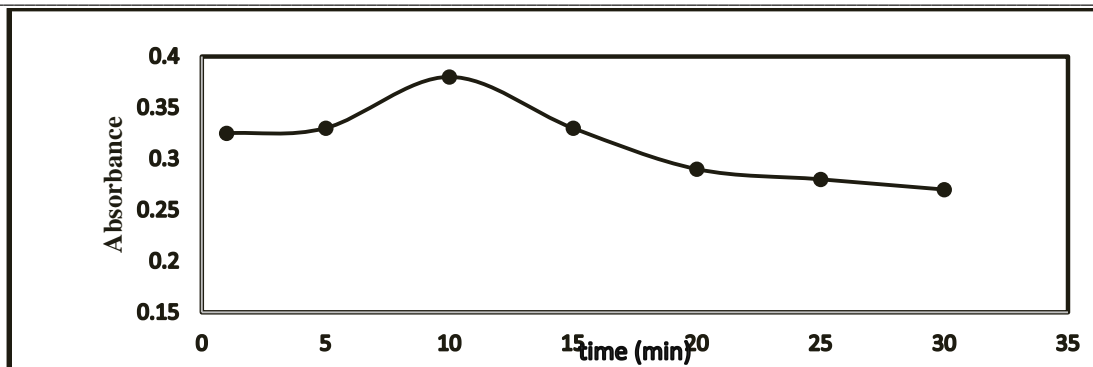


Fig. 12: Effect of time on the complexes formed between reagent 4b and metal ion.

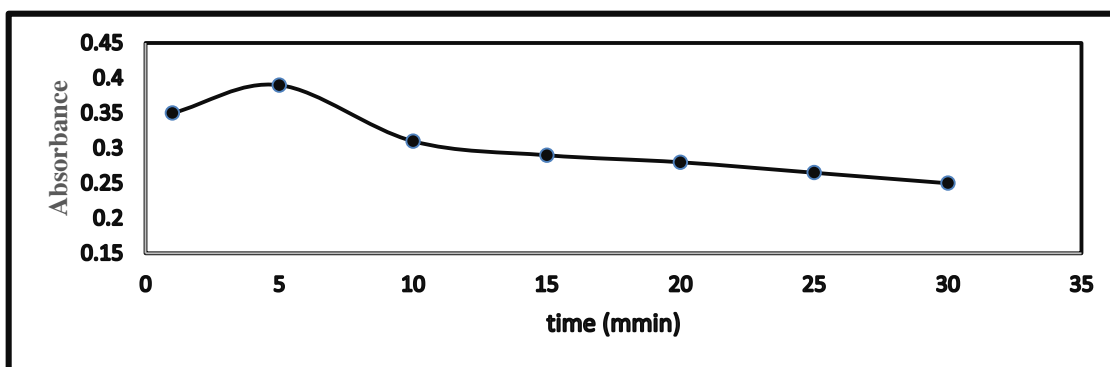


Fig. 13: Effect of time on the complexes formed between reagent 4c and metal ion.

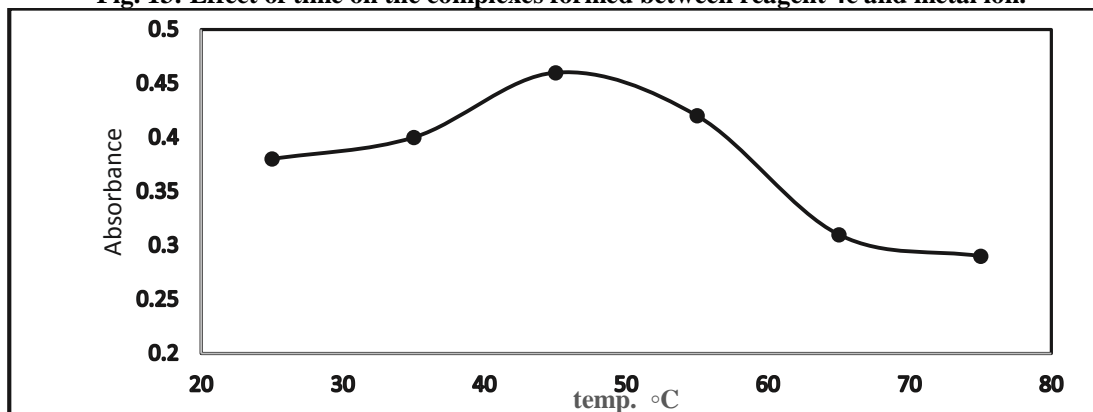


Fig. 14: Effect of temperature on the complex formed between reagent 4b and metal ions.

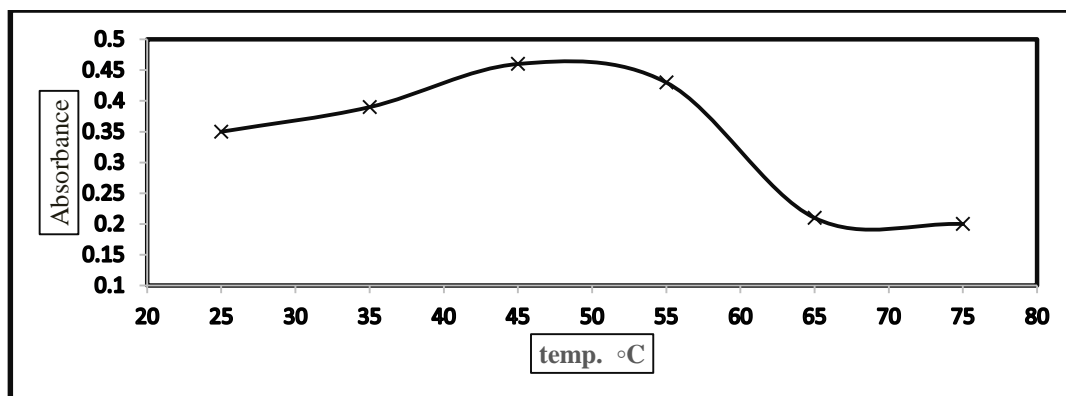


Fig. 15: Effect of temperature on the complex formed between reagent 4bc and metal ions.

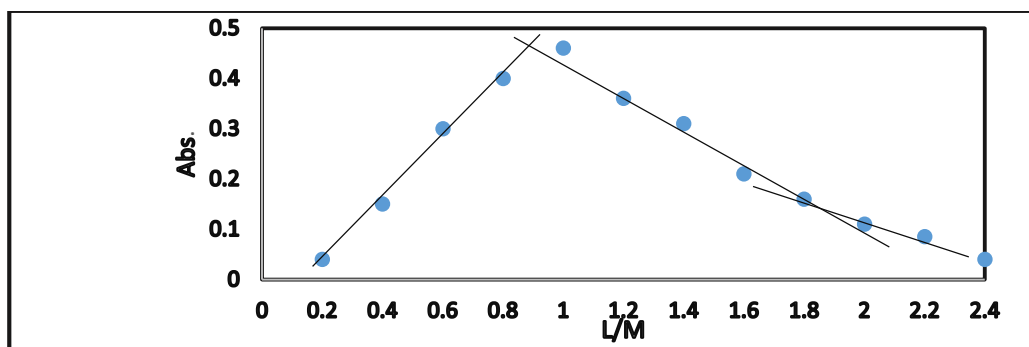


Fig. 16: Molar ratio of reagent 4b using (1.0 mL of  $5.0 \times 10^{-3} \text{M}$ ) of metal ions at optimum conditions for the complex under consideration.

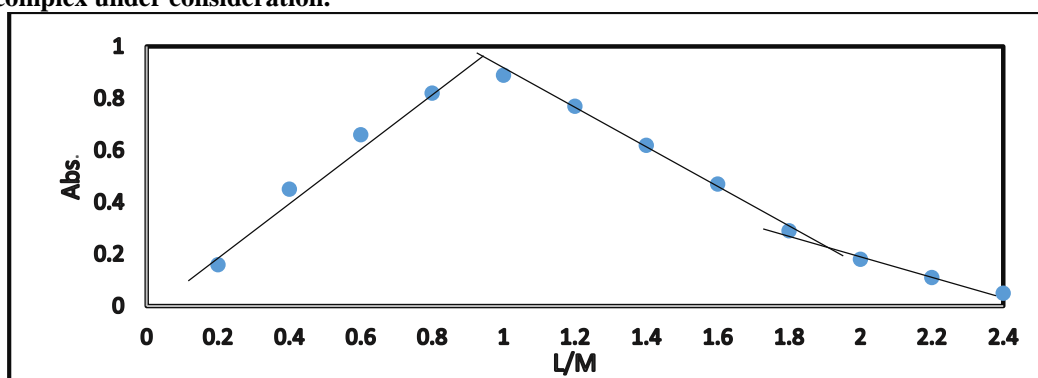


Fig. 17: Molar ratio of reagent 4c using (1.0 mL of  $5.0 \times 10^{-3} \text{M}$ ) of metal ions at optimum conditions for the complex under consideration.

### 3.6. Obevence of Beer's Law

The obevence of  $\text{Co}^{2+}$  complexes with reagent 4b and 4c to Beer's law was verified in order to use such complexes for their spectrophotometric determination. Representative plots of Beer are given in Fig. 18, 19. The molar absorptivity ( $\epsilon$ ) values expressed in ( $\text{L mol}^{-1} \text{cm}^{-1}$ ) were obtained as the slopes of the constructed calibration curves lines from which

the specific absorptivity ( $a$ ) ( $\text{L g}^{-1} \text{cm}^{-1}$ ) [30-32], corresponding to the absorbance of  $1 \mu\text{g mL}^{-1}$  in a cuvette with an optical path length of 1 cm. Beer's law was verified and found to be satisfactory obeyed for the concentration ranges 1-9 and  $0.5\text{-}6.5 \mu\text{g mL}^{-1}$  for  $\text{Co}^{2+}$  - (4b) and  $\text{Co}^{2+}$  - (4c) complexes, respectively. The RSD for six replicate measurements  $\text{Co}^{2+}$  - (4b) and  $\text{Co}^{2+}$  - (4c) were 1.35 and 2.8%, respectively.

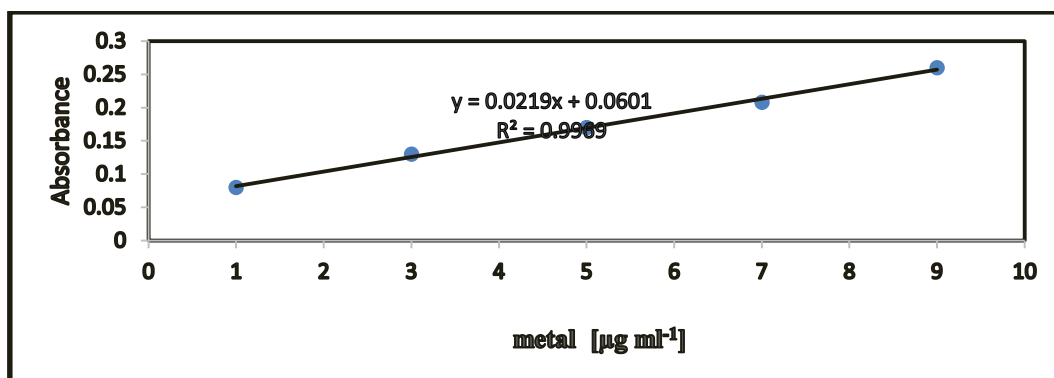


Fig. 18: Application of Beer's law for studied complex using the optimum conditions of reagent 4b

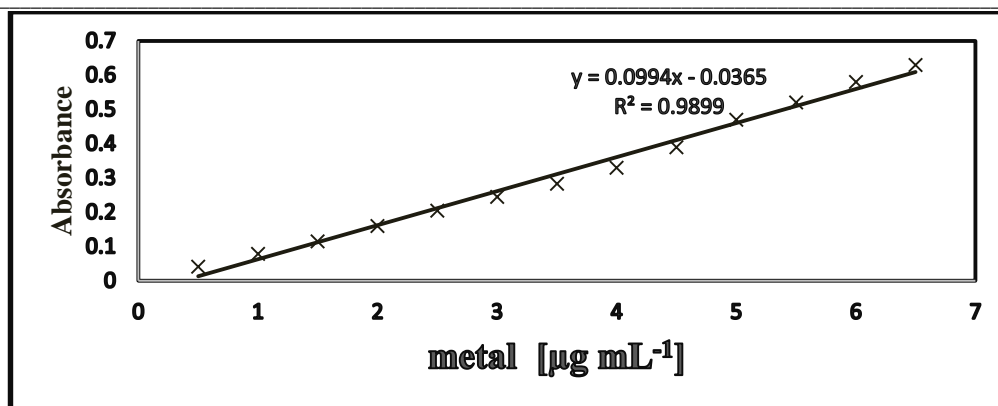


Fig. 19: Application of Beer's law for studied complex using the optimum conditions of reagent 4c.

### 3.7. Fluorescence Measurements

#### A- Fluorescence measurements of (4b-c)

##### ligands

Compounds 4b and 4c showed very good fluorescence properties with large Stokes' shift even before adding the metal salts and forming the complex, which is very important in super-resolution optical microscopy of biological objects. Two different instruments were used to measure  $\lambda_{Abs}$  and  $\lambda_{Ex}$ , there

was 1-3 nm difference between the two measurements Table 1.

#### B- Fluorescence measurements of (4b-c) complexes.

Compounds 4b and 4c exhibited improvement in their fluorescence properties after adding the metal salts and forming the complex. Two different instruments were used to measure  $\lambda_{Abs}$  and  $\lambda_{Ex}$ , so there was 1-3 nm difference between the two measurements Table 2.

Table 1. : The fluorescence properties of 4b and 4c ligands.

| Comp. | $\lambda_{Abs}$ | $\lambda_{Ex}$ | $\lambda_{Em}$ | Stokes's shift in nm     |
|-------|-----------------|----------------|----------------|--------------------------|
| 4b    | 367 nm          | 385 nm         | 428 nm         | 43 nm bathochromic shift |
| 4c    | 391 nm          | 385 nm         | 463 nm         | 78 nm bathochromic shift |

Table 2. : The fluorescence properties of 4b and 4c complexes.

| Comp. | $\lambda_{Abs}$ | $\lambda_{Ex}$ | $\lambda_{Em}$ | Stokes's shift in nm     |
|-------|-----------------|----------------|----------------|--------------------------|
| 4b    | 402 nm          | 459 nm         | 540 nm         | 80 nm bathochromic shift |
| 4c    | 439 nm          | 438 nm         | 467 nm         | 29 nm bathochromic shift |

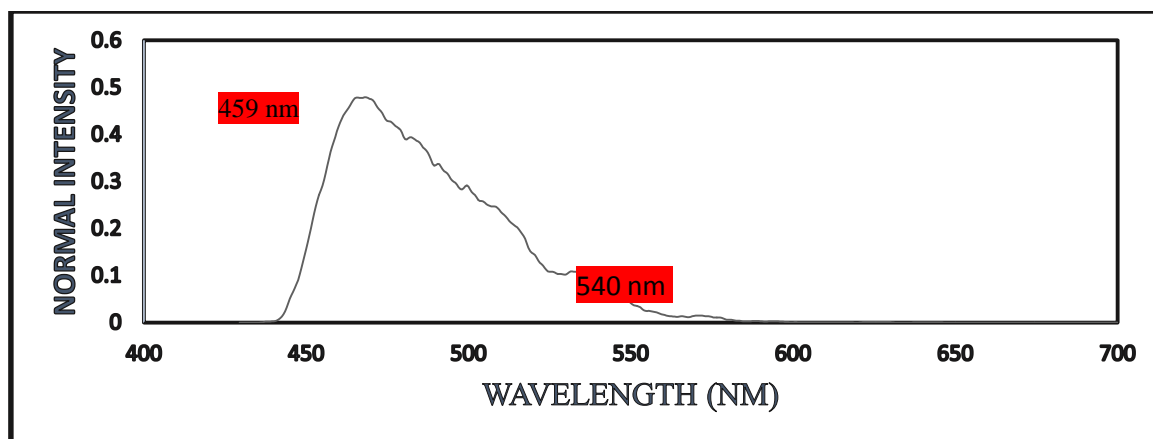
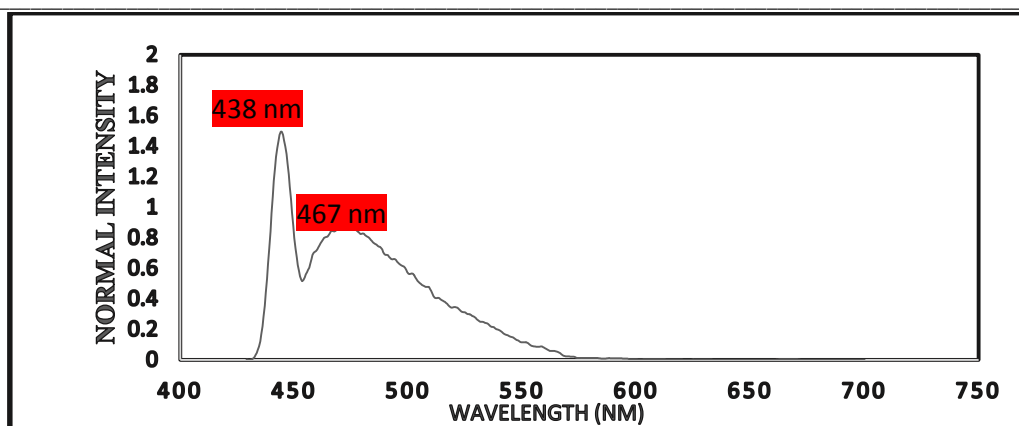


Fig. 20. Emission spectra for 4b-complex.



**Fig. 21. Emission spectra for 4cb-complex.**

### Conclusion

We developed novel compounds that can mimic the natural GFP chromophore and possess sites suitable for complexation with transitional metals. The chemical structure of these compounds was confirmed by <sup>1</sup>H-NMR and IR. The photophysical properties of these compound was studied to evaluate their ability to produce fluorescence and they showed very good fluorescence properties. These compounds were tested for their ability to make complexes with different transition metals and they showed very good chelation activity toward cobalt.

### References:

- Robinson, B. W. *et al.* Recent advances in molecular biological techniques and their relevance to pulmonary research. *Thorax* **55**, 329–39 (2000).
- Larkin, P. D. & Hartberg, Y. Development of a green fluorescent protein-based laboratory curriculum. *Biochem. Mol. Biol. Educ.* **33**, 41–45 (2005).
- Guan, Y. *et al.* Live-cell multiphoton fluorescence correlation spectroscopy with an improved large Stokes shift fluorescent protein. *Mol. Biol. Cell* **26**, 2054–2066 (2015).
- Lee, J.-Y. & Kitaoka, M. A beginner's guide to rigor and reproducibility in fluorescence imaging experiments. *Mol. Biol. Cell* **29**, 1519–1525 (2018).
- Heppert, J. K. *et al.* Comparative assessment of fluorescent proteins for in vivo imaging in an animal model system. *Mol. Biol. Cell* **27**, 3385–3394 (2016).
- Thorn, K. Genetically encoded fluorescent tags. *Mol. Biol. Cell* **28**, 848–857 (2017).
- Lee, S. *et al.* DNA binding fluorescent proteins for the direct visualization of large DNA molecules. *Nucleic Acids Res.* **44**, e6 (2016).
- Remington, S. J. Green fluorescent protein: a perspective. *Protein Sci.* **20**, 1509–19 (2011).
- Kaishima, M., Ishii, J., Matsuno, T., Fukuda, N. & Kondo, A. Expression of varied GFPs in *Saccharomyces cerevisiae*: codon optimization yields stronger than expected expression and fluorescence intensity. *Sci. Rep.* **6**, 35932 (2016).
- Zimmer, M. Green fluorescent protein (GFP): Applications, structure, and related photo physical behavior. *Chem. Rev.* **102**, 759–781 (2002).
- Lippincott-Schwartz, J. & Patterson, G. H. Development and use of fluorescent protein markers in living cells. *Science*. **300**, 87–91 (2003).
- Chalfie, M., Tu, Y., Euskirchen, G., Ward, W. W. & Prasher, D. C. Green fluorescent protein as a marker for gene expression. *Science*. **263**, 802–805 (1994).
- Huh, W. K. *et al.* Global analysis of protein localization in budding yeast. *Nature* **425**, 686–691 (2003).
- Fehr, M., Frommer, W. B. & Lalonde, S. Visualization of maltose uptake in living yeast cells by fluorescent nanosensors. *Proc. Natl. Acad. Sci.* **99**, 9846–9851 (2002).
- Davenport, D. & Nicol, J. A. C. Luminescence in Hydromedusae. *Proc. R. Soc. B Biol. Sci.* **144**, 399–411 (1955).
- Shimomura, O., Johnson, F. H. & Saiga, Y. Extraction, Purification and Properties of Aequorin, a Bioluminescent Protein from the Luminous Hydromedusan, *Aequorea*. *J. Cell. Comp. Physiol.* **59**, 223–239 (1962).
- Shimomura, O. The discovery of aequorin and green fluorescent protein. *J. Microsc.* **217**, 3–15 (2005).
- Hastings, J. W. Biological diversity, chemical mechanisms, and the evolutionary origins of bioluminescent systems. *J. Mol. Evol.* **19**, 309–321 (1983).
- Rees, J. *et al.* The Origins of Marine Bioluminescence: Turning Oxygen Defence

- Mechanisms Into Deep-Sea Communication Tools. *J. Exp. Biol.* **201**, 1211–1221 (1998).
20. Niwa, H. *et al.* Chemical nature of the light emitter of the *Aequorea* green fluorescent protein. *Proc. Natl. Acad. Sci. U. S. A.* **93**, 13617–22 (1996).
  21. Nishiuchi, Y. *et al.* Chemical synthesis of the precursor molecule of the *Aequorea* green fluorescent protein, subsequent folding, and development of fluorescence. *Proc. Natl. Acad. Sci. U. S. A.* **95**, 13549–54 (1998).
  22. Tsien, R. Y. The Green Fluorescent Protein. *Proteins* **67**, 509–44 (1998).
  23. Poppe, L. Methylidene-imidazolone: A novel electrophile for substrate activation. *Current Opinion in Chemical Biology* **5**, 512–524 (2001).
  24. Schwede, T. F., Rétey, J. & Schulz, G. E. Crystal structure of histidine ammonia-lyase revealing a novel polypeptide modification as the catalytic electrophile. *Biochemistry* **38**, 5355–5361 (1999).
  25. Orm, M. *et al.* Crystal Structure of the *Aequorea victoria* Green Fluorescent Protein. *Science*. **273**, 1392–1395 (1996).
  26. Yang, F., Moss, L. G. & Phillips, G. N. The molecular structure of green fluorescent protein. *Nat. Biotechnol.* **14**, 1246–1251 (1996).
  27. Morise, H., Shimomura, O., Johnson, F. H. & Winant, J. Intermolecular energy transfer in the bioluminescent system of *Aequorea*. *Biochemistry* **13**, 2656–2662 (1974).
  28. Kremers, G.-J., Gilbert, S. G., Cranfill, P. J., Davidson, M. W. & Piston, D. W. Fluorescent proteins at a glance. *J. Cell Sci.* **124**, 2676–2676 (2011).
  29. Yampolsky, I. V *et al.* Synthesis and properties of the red chromophore of the green-to-red photoconvertible fluorescent protein Kaede and its analogs. *Bioorg. Chem.* **36**, 96–104 (2008).
  30. Plöchl, J. Ueber Phenylglycidäure (Phenyloxacrylsäure). *Berichte der Dtsch. Chem. Gesellschaft* **16**, 2815–2825 (1883).
  31. Jun, E. E. Ueber die Condensation der Hippursäure mit Phtalsäureanhydrid und mit Benzaldehyd. *Justus Liebig's Ann. Der Chemie* **275**, 1–8 (1893).
  32. Voliani, V. *et al.* Cis - Trans Photo isomerization of Fluorescent Protein Chromophores. *J. Phys. Chem. B* **112**, 10714–10722 (2008).
  33. Huang, G. J. *et al.* Effects of hydrogen bonding on internal conversion of GFP-like chromophores. I. the para-amino systems. *J. Phys. Chem. B* **117**, 2695–2704 (2013).